LIGHTCURVE AND CONSTRAINTS ON THE SPIN VECTOR OF KORONIS FAMILY MEMBER (1840) HUS: ILLUSTRATING ANALYSIS OF A COMBINED DATA SET

Stephen M. Slivan, Claire J. McLellan-Cassivi
Massachusetts Institute of Technology
Dept. of Earth, Atmospheric, and Planetary Sciences
77 Mass. Ave. Rm. 54-424, Cambridge, MA 02139
slivan@mit.edu

Miquel Serra-Ricart, M.R. Alarcón
Instituto de Astrofísica de Canarias
La Laguna, Tenerife, Spain

(Received: 2023 April 10)

A new lightcurve of Koronis asteroid family member (1840) Hus records two consecutive rotations and confirms the resolution by Slivan et al. (2021) of the rotation period alias. The data are analyzed together with additional new lightcurves (Fornas et al., 2023) as well as observations from earlier apparitions as a case study to illustrate a spin vector determination described in detail, and as an example of an analysis that is documented so that a reader can understand what level of confidence is merited for the results. The Hus data set yields an unambiguous count of rotations back to 2001, a sidereal rotation period of 4.749052 ± 0.000002 h, and indicates that the spin is prograde with a high-latitude pole.

The rotation period determination for Koronis family member (1840) Hus reported by Slivan et al. (2021) was identified as being the only solution that is consistent with the published lightcurve observations, but suitable single-night coverage of a full rotation period was not available to directly check the result. During its apparition in 2023, Hus was observed to obtain a low-noise lightcurve recording nearly two consecutive rotations on a single night which confirms the period. Also, during the same apparition in 2023, Fornas et al. (2023) observed Hus during three lunations to more precisely determine a synodic rotation period. This paper documents in detail as a case study an analysis of all of the 2023 data together with observations from previous apparitions to count sidereal rotations, determine the sense of spin and sidereal rotation period, and constraints on the spin vector orientation, including at each step an assessment of the suitability of the data set to proceed.

Hus was observed on the night of UT 2023 Jan 23-24 at the Teide Observatory at Tenerife, Spain as part of a project during the MIT Astronomy Field Camp subject, using an 0.8-m testing telescope for the Two-Meter Twin Telescope (TTT) project. An Andor iKon-L 936 CCD camera was mounted at a Nasmyth focus, imaging a 17′×17′ field for an unbinned image scale of 0.51 arcsec/pix. Image integrations were 60 s using an *r′* filter. The images were processed for bias, dark, and flat corrections using the TTT data pipeline, and measured using *AstroImageJ* (Collins et al., 2017). A comparison star from the APASS DR9 catalog (Henden et al., 2015) comparable to solar color was used to determine the zero-point calibration to *r′* magnitudes. The resulting lightcurve (Fig. 1) was reduced for light-time and to unit distances. The single-night observed span of 9.0 h records just over 1.9 rotations for unambiguous redundant coverage in rotation phase, yielding a synodic rotation period of 4.75 ± 0.02 h and confirming the alias resolution of Slivan et al. (2021).

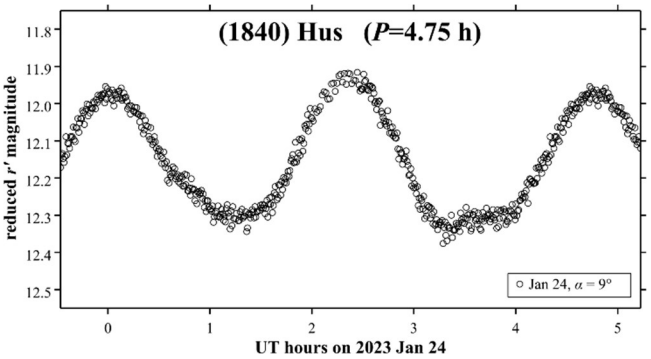

Figure 1. Folded composite lightcurve of (1840) Hus during its 2023 apparition, light-time corrected, showing one rotation period plus the earliest and latest 10% repeated. The estimated error in the *r′* zero-point calibration is 0.03 mag. The legend gives UT date of observation and solar phase angle *α*.

The observations of Hus in 2023 comprise its third apparition of dedicated lightcurves, recording a viewing aspect not included among the published lightcurves from the apparitions observed in 2009 (Clark, 2010) and 2020 (Slivan et al., 2021). The calculation given by Slivan (2012; Eqs. 3-5) can be used to test whether the previously published synodic period is precise enough to unambiguously count rotations between the closest-in-time observed apparitions in the data set, which are those in 2020 and 2023. For $\sigma_{99}(P_{syn})$ = 0.002 h and P_{syn} = 4.748 h with the epochs given in Table I, Δt = 21554 h and the result is an ambiguity among N_{per} = 9 possible solutions. However, during its 2023 apparition Hus also was observed by Fornas et al. (2023) who recorded data spanning three lunations to maximize the precision of the derived synodic rotation period. Combining all of the 2023 data for analysis gives a derived synodic period of 4.7491 ± 0.0001 h, for $\sigma_{99}(P_{syn})$ = 0.00025 h and N_{per} = 1 solution indicating that an unambiguous rotation count between the two apparitions has been achieved.

The next test is whether the rotation counting can be expanded across the entire data set, in this case back to the epoch from 2009. In this context it is important that the uncertainties of the epochs be carefully estimated. The epoch errors given in Table I are based on the RMS error of the corresponding unfiltered Fourier series fit model to the lightcurve data, calculating the corresponding error along the time axis by dividing by the steepest slope on the filtered model; that is, the slope at its mean value crossing. Using these error estimates, the "sieve algorithm" of Slivan (2013) reveals that the sidereal rotation count from 2009 to 2023 is indeed unambiguous (Fig. 2).

Having confirmed that the data set satisfies both rotation-counting tests, the third test is to see whether the available data can also begin to constrain the spin pole orientation by distinguishing whether the direction of spin is prograde or retrograde; that is, identify whether the spin pole lies in the northern or the southern ecliptic hemisphere, respectively. Constraining pole location involves greater demands on the data set, and three viewing geometries is too few to provide enough information for a credible result. To proceed, the Minor Planet Center Orbits/Observations Database was searched for photometry of Hus that yields suitable composite lightcurves from additional apparitions. Lightcurves from the apparitions in 2019 (similar aspect to the noisy data from 2009) and in 2021 (an aspect lacking dedicated lightcurves) were assembled from data recorded by the ATLAS sky survey (Tonry et al., 2018) and are shown in the upper panels of Fig. 3. The polar graph of the corresponding phase angle bisector (PAB) longitudes in Fig. 4 shows an unusually

symmetric pattern of longitudes always close to 90 degrees apart; this is a consequence of the asteroid's orbit period 4.98 years being nearly 5:1 commensurate with Earth's orbit period, and means that the data set lacks observations from intermediate longitudes having information to break the symmetry and distinguish the direction of spin. A second consequence is that the viewing aspect changes by only a small angle for each successive asteroid orbit (2 to 3 degrees per decade for two orbits), so that multiple asteroid orbits must elapse to assemble coverage of intermediate longitudes. The MPC Database then was checked specifically for additional suitable lightcurves of Hus from apparitions as far back in time as possible, in order to maximize the differences in PAB longitude from the most recent apparitions. Usable composite lightcurves from the apparitions in 2001 in 2003 were assembled from data recorded at the USNO Flagstaff station and are shown in the lower panels of Fig. 3.

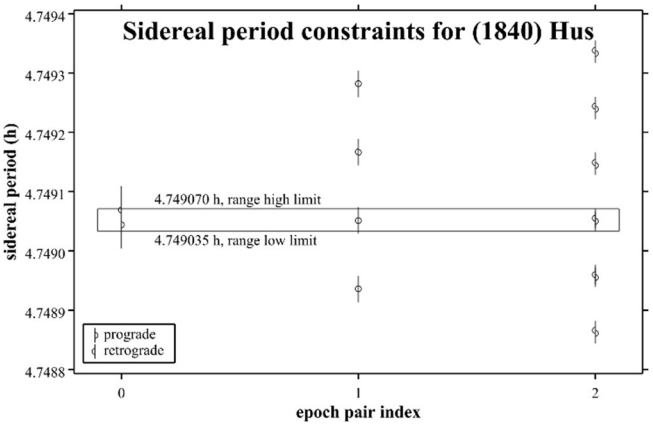

Figure 2. Ranges of possible sidereal rotation periods allowed by the three epochs in Part A of Table I. Each horizontal coordinate index represents the time interval between a pair of epochs (Table II), with longer intervals to the right. Points and range bars represent sidereal periods calculated from every possible number of rotations that could elapse during the interval. The thin horizontal rectangle identifies the single range of periods that is allowed by all three time intervals.

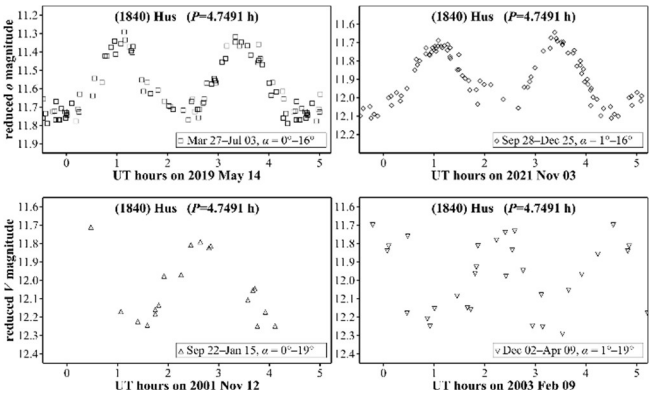

Figure 3. Composite lightcurves of data from sky surveys. (Upper panels) Reduced *o*-band data from ATLAS, selecting the subsets of data points that were recorded between the stationary points of the apparitions. The slope parameter G_o values used to reduce for changing solar phase angle, 0.23 for 2019 and 0.26 for 2021, were determined from the data by fitting the Lumme-Bowell model (Bowell et al., 1989) using the approach described by Slivan et al. (2008). (Lower panels) Reduced *V*-band data from USNO Flagstaff Station. The slope parameter G = 0.23 for S-type objects (Lagerkvist and Magnusson, 1990) was used to reduce for changing solar phase angle.

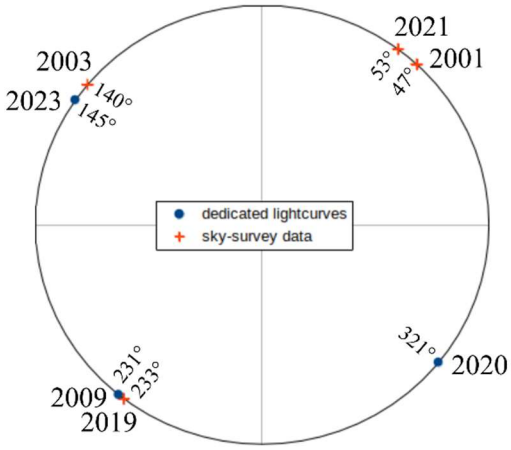

Figure 4. Angular distribution of ecliptic longitudes of PABs for epochs in Table I. Each apparition of sky survey data is represented by a single longitude calculated for the "median date" of the UT dates of observations, reflecting that the information content of these data comes from the nights in combination rather than each night taken individually.

Sidereal photometric astrometry (SPA) (Slivan, 2014; Drummond et al., 1988) was used to calculate the contour graph in Fig. 5 from the expanded set of all seven epochs, which indicates prograde spin and a high ecliptic latitude for the pole. Information about the pole longitude is less clear, partly because longitudes from epoch analyses can be subject to systematic errors even for a plentiful data set, and partly because in this case the symmetry of the observing aspect coverage in ecliptic longitude skews the pattern of contours. The ambiguity of the two pole regions cannot be resolved by the lightcurves because of the small orbit inclination of Hus, about 2 degrees. Crudely estimating from the pole regions graph in Fig. 5, the pole solution P_1 latitude is about +70°, longitude between about 335° and 35°; solution P_2 latitude is about +74°, longitude between about 165° and 225°. In the absence of a clear pole solution, the most secure sidereal period result comes from applying the sieve algorithm to the expanded set of all seven epochs in Table I, which yields 4.749052 ± 0.000002 h for prograde rotation. A summary of the results is presented in Table III, in which the estimated ranges of the pole longitudes are represented as larger uncertainties, and the coarse estimate of the *a*/*b* axial ratio is based on a triaxial ellipsoid model. The poor constraint on pole longitudes limits the possibilities for more meaningful shape modeling; in particular, the restricted set of viewing geometries falls short of what would be needed for reliable pole and shape model results from convex inversion.

The published sidereal period result that Ďurech et al. (2016) determined for Hus using an ellipsoidal model shape satisfies the same rotation count constraint determined in this work using the sieve algorithm, but the retrograde period value corresponds to an alias sidereal period from our analysis. The accompanying single pole solution that they obtained using convex inversion (Kaasalainen et al., 2001) is about 150° away in pole latitude from our solutions in the opposite ecliptic hemisphere, and thus is not consistent with the constraints from the epochs analysis.

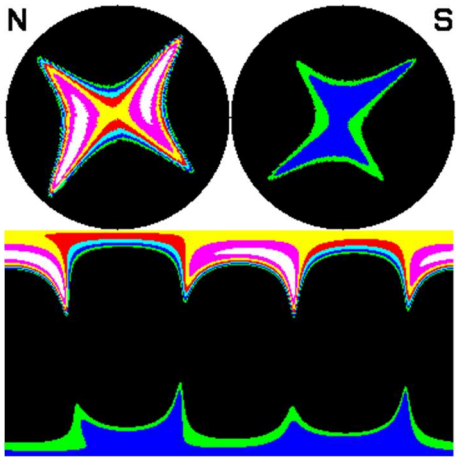

Figure 5. Contour graphs of RMS error of trial poles for the SPA analyses of the seven epochs in Table I. In the lower half of the figure the celestial sphere is projected on a rectangular grid of ecliptic longitude and latitude; the same data in a polar format undistorted near the ecliptic poles appear in the upper half of the graph where north and south hemispheres are plotted separately. Best-fit regions are colored white. The results locate a symmetric pair of high-latitude prograde pole regions, although the skewed pattern of contours also reflects the very incomplete observing aspect coverage in ecliptic longitude.

UT date	Epoch (UT h)	PAB λ,β(°)	Data ref.
Part A: Dedicated lightcurves			
2009 Jun 15	1.89 ± 0.35	230.8 -0.8	a
2020 Aug 09	0.80 ± 0.11	321.1 -3.0	b
2023 Jan 24	2.39 ± 0.03	145.4 +2.9	c
Part B: Sky survey lightcurves sparse-in-time			
2001 Nov 12	2.69 ± 0.14	47.0 +0.4	d
2003 Feb 09	2.23 ± 0.21	140.3 +3.0	d
2019 May 14	3.46 ± 0.07	232.5 -0.6	e,f
2021 Nov 03	3.47 ± 0.07	53.2 +0.5	e,f

Table I. Summary of lightcurve epochs, in each case locating a maximum from the second harmonic of a Fourier series model fit to the lightcurves. PAB λ,β are the J2000.0 ecliptic longitude and latitude of the phase angle bisector. Data references are a, Clark (2010); b, Slivan et al. (2021); c, this work; d, USNO Flagstaff station; e, ATLAS-MLO *o*-band; f, ATLAS-HKO *o*-band. Photometry from USNO Flagstaff and from the ATLAS survey was retrieved from the MPC Orbits/Observations Database.

Epoch pair index	Interval (d)	Interval (app.)	Epochs source apparitions
0	898.1	2	2020, 2023
1	4073.0	9	2009, 2020
2	4971.0	11	2009, 2023

Table II. Time intervals between lightcurve epochs used to identify the ranges of possible sidereal periods in Fig. 2. Columns are: epoch pair index label in Fig. 2, interval length rounded to 0.1 d, the corresponding integer count of elapsed apparitions, and the apparitions from which the defining epochs were measured.

		λ(°)	β(°)
sidereal period:	4.749052 ± 0.000002 h		
spin poles:	P_1	5 ± 15	+70 ± 5
	P_2	195 ± 15	+74 ± 5
model axial ratio a/b:	~1.4		

Table III. Summary of period and pole results. The errors for the pole coordinates are given in degrees of arc and were estimated based on the RMS error distribution of the SPA fits to trial poles.

Acknowledgments

We thank Dr. Michael Person for organizing and conducting the Field Camp, and G. Fornas for providing his data prior to publication. This article includes observations made at the Two-Meter Twin Telescope (TTT) at the Teide Observatory (managed by the Instituto de Astrofísica de Canarias) that Light Bridges, SL, operates on the Island of Tenerife, Canary Islands (Spain). This research has made use of the VizieR catalogue access tool, CDS, Strasbourg, France (*DOI:10.26093/cds/vizier*). This work also has made use of data and services provided by the International Astronomical Union's Minor Planet Center; specifically, the brightnesses accompanying astrometry from the USNO Flagstaff station and from the Asteroid Terrestrial-impact Last Alert System (ATLAS) survey observing program.

References

Bowell, E.; Hapke, B.; Domingue, D.; Lumme, K.; Peltoniemi, J.; Harris, A.W. (1989). "Application of Photometric Models to Asteroids." In *Asteroids II* (R.P. Binzel; T. Gehrels; M.S. Matthews, eds.) pp. 524-556. Appendix: The IAU Two-Parameter Magnitude System for Asteroids. U. of Arizona Press, Tucson, AZ.

Clark, M. (2010). "Asteroid Lightcurves from the Chiro Observatory." *Minor Planet Bull.* **37**, 89-92.

Collins, K.A.; Kielkopf, J.F.; Stassun, K.G.; Hessman, F.V. (2017). "AstroimageJ: Image Processing and Photometric Extraction for Ultra-precise Astronomical Light Curves." *Astron. J.* **153**, A77.

Drummond, J.D.; Weidenschilling, S.J.; Chapman, C.R.; Davis, D.R. (1988). "Photometric geodesy of main-belt asteroids. II. Analysis of lightcurves for poles, periods, and shapes." *Icarus* **76**, 19-77.

Ďurech, J.; Hanuš, J.; Oszkiewicz, D.; Vančo, R. (2016). "Asteroid Models from the Lowell Photometric Database." *Astron. Astrophys.* **587**, A48.

Fornas, G.; Fornas, A.; Arce, E.; Huet, F. (2023). "Lightcurve Analysis of the Koronis Family Member 1840 Hus." *Minor Planet Bull.* **50**, 189.

Henden, A.A.; Levine, S.; Terrell, D.; Welch, D.L. (2015). "APASS - The Latest Data Release." *American Astronomical Society 225th Meeting*, id 336.16.

Number	Name	yyyy mm/dd	Phase	L_{PAB}	B_{PAB}	Period(h)	P.E.	Amp	A.E.
1840	Hus	2023 01/24-01/24	8.7	145	3	4.75	0.02	0.40	0.02

Table IV. Observing circumstances and results. Phase is the solar phase angle. L_{PAB} and B_{PAB} are the approximate phase angle bisector longitude and latitude.

Kaasalainen, M.; Torppa, J.; Muinonen, K. (2001). "Optimization methods for asteroid lightcurve inversion. II. The complete inverse problem." *Icarus* **153**, 37-51.

Lagerkvist, C.I.; Magnusson, P. (1990). "Analysis of asteroid lightcurves. II. Phase curves in a generalized HG-system." *Astron. Astrophys. Suppl.* **86**, 119-165.

Slivan, S.M.; Binzel, R.P.; Boroumand, S.C.; Pan, M.W.; Simpson, C.M.; Tanabe, J.T.; Villastrigo, R.M.; Yen, L.L.; Ditteon, R.P.; Pray, D.P.; Stephens, R.D. (2008). "Rotation Rates in the Koronis Family, Complete to $H \approx 11.2$." *Icarus* **195**, 226-276.

Slivan, S.M. (2012). "Epoch Data in Sidereal Period Determination. I. Initial Constraint from Closest Epochs." *Minor Planet Bull.* **39**, 204-206.

Slivan, S.M. (2013). "Epoch data in sidereal period determination. II. Combining epochs from different apparitions." *Minor Planet Bull.* **40**, 45-48.

Slivan, S.M. (2014). "Sidereal Photometric Astrometry as Efficient Initial Search for Spin Vector." *Minor Planet Bull.* **41**, 282-284.

Slivan, S.M.; McLellan-Cassivi, C.; Shishido, R.; Wang, N. (2021). "Rotation Period of Koronis Family Member 1840 Hus." *Minor Planet Bull.* **48**, 112-113.

Tonry, J.L.; Denneau, L.; Heinze, A.N.; Stalder, B.; Smith, K.W.; Smartt, S.J.; Stubbs, C.W.; Weiland, H.J.; Rest, A. (2018). "ATLAS: A High-cadence All-sky Survey System." *PASP* **130**, 064505.

AN IMPROVED LIGHTCURVE AND ROTATION PERIOD OF 1178 IRMELA

Frederick Pilcher
Organ Mesa Observatory (G50)
4438 Organ Mesa Loop
Las Cruces, NM 88011 USA
fpilcher35@gmail.com

Lorenzo Franco
Balzaretto Observatory (A81), Rome, ITALY

Giulio Scarfi
Iota Scorpii Observatory (K78), La Spezia, ITALY

Paolo Bacci, Martina Maestripieri
GAMP - San Marcello Pistoiese (104), Pistoia, ITALY

Paolo Fini, Guido Betti
Beato Ermanno Astronomical Observatory (L73)
Impruneta, ITALY

Alessandro Marchini
Astronomical Observatory, University of Siena (K54)
Via Roma 56, 53100 - Siena, ITALY

(Received: 2023 Feb 26)

A collaboration of observers from North America and Europe has produced a lightcurve of 1178 Irmela with synodic period 11.992 ± 0.001 hours, amplitude 0.29 ± 0.02 magnitudes, and full phase coverage.

Previously published period determinations for 1178 Irmela are reported by Binzel (1987), 19.17 hours; Stephens (2012), 11.989 hours; and Polakis (2019), 11.985 hours. The lightcurves published by Stephens (2012) and by Polakis (2019) were made from a single observatory and therefore show only about 2/3 phase coverage for an Earth-commensurate period. Stephens (2012) showed that the 19.17-hour period published by Binzel (1987), based upon sparse lightcurves widely spaced in time, is an 8/5 alias of a period near 11.99 hours.

The authors of this paper, widely spaced in longitude in North America and Europe, respectively, agreed to collaborate to obtain full phase coverage. An equipment list for all observers is provided in table II. Ten sessions 2023 Jan. 26 - Feb. 17 provide a very good fit to bimodal lightcurve with synodic period 11.992 ± 0.001 hours and amplitude 0.29 ± 0.02 magnitudes with full phase coverage. This result is very close to the periods published by Stephens (2012) and by Polakis (2019), and to 5/8 of the period by Binzel (1987).

On 2023 Jan. 31, P. Bacci and M. Maestripieri obtained alternating data points in the V and R filters that show V-R = 0.40. This value is within the usual range 0.38 ± 0.05 for asteroids with C-type taxonomic classifications (Shevchenko and Lupishko, 1998).